Quantum magnetoresistance fluctuations in an amorphous metal

W. F. Smith,* T. S. Tighe, G. C. Spalding,† M. Tinkham, and C. J. Lobb‡
Department of Physics and Division of Applied Sciences, Harvard University, Cambridge, Massachusetts 02138
(Received 18 January 1991)

We report an observation of aperiodic magnetoresistance fluctuations in an amorphous system. We have observed fluctuations in amorphous $Pd_{80}Si_{20}$ wires with macroscopic lengths, up to $L=1$ mm ($L/L_\varphi=12\,000$, where L_φ is the phase-coherence length). The root-mean-square amplitude of the resistance fluctuations is proportional to $L^{1/2}$, in agreement with theory. We observe a reduction in the fluctuation amplitude at low magnetic fields, which we attribute to magnetic scattering, possibly in the Kondo regime. Two simple models are presented to describe this behavior, one based on a single population of magnetic scatterers with temperature-dependent magnetic moment, and the other based on two scatterer populations, each with fixed moment. Both models agree with the data. We use the high-field amplitude of the magnetoresistance-fluctuation structure to predict the characteristic field scale; the prediction is larger than the observed field scale by a factor of 2.

I. INTRODUCTION

Aperiodic but reproducible fluctuations in the magnetoresistance of mesoscopic wires were discovered accidentally in the search for the Aharonov-Bohm (AB) effect in normal metals.[1] These "quantum conductance fluctuations" (QCF's) are a striking manifestation of the wave nature of conduction electrons, as can be seen from the following simple argument.[2] A conduction electron traversing the length of a wire undergoes many elastic scattering events, but, for small samples at low temperatures, the electron remains at constant energy, and so maintains phase coherence. Therefore quantum-mechanical interference occurs between the possible diffusive Feynman paths through the sample. An applied perpendicular magnetic field threads through the many loops enclosed between the various paths, causing an Aharonov-Bohm interference shift, which changes the transmission probability of the electron and therefore the resistance of the sample. Because there are many loops, each of random area, the resistance fluctuates aperiodically as the magnetic field is swept up. But, since the areas of the loops are constant, this aperiodic pattern reproduces as the field is swept back down. If a scattering site is moved, all paths having that site as a vertex will change, and the magnetoresistance pattern will change. Since the positions of scattering sites differ from one sample to another, even if the samples are nominally identical, the magnetoresistance trace is called the "magnetofingerprint" (MF).

MF's have been observed in polycrystalline metals and semimetals, and in semiconductors.[3] Previous studies on the length dependence of the resistance-fluctuation structure[4] have examined the regime $L \lesssim 30L_\varphi$ ($L \lesssim 6L_\varphi$ for metallic samples[5]), where L is the sample length and L_φ is the diffusion length over which the conduction electrons maintain phase coherence.

In this paper, we present the first data showing MF's in an amorphous system, $Pd_{80}Si_{20}$. Our data demonstrate that this phenomenon does not require the conduction electrons to be in Bloch states, or, equivalently in real space, that it can take place in the extreme diffusion limit, where the elastic mean free path l is on the order of the interatomic spacing. From a structural viewpoint, the amorphous and polycrystalline states are qualitatively different. For purposes of electrical conduction, it is not clear whether the difference is qualitative or merely a matter of degree.[6] Our results indicate that, as far as QCF's are concerned, the states are similar, since the QCF theory previously applied to polycrystalline systems also explains our results.

We have also studied the transition to more classical behavior by measuring resistance fluctuations of samples with L up to 1 mm ($L \cong 12\,000\ L_\varphi$). The theory of stochastic averaging[2] predicts that the fluctuations should be observable in this regime; in fact, the amplitude of the resistance fluctuations should *increase* proportional to $L^{1/2}$ (although the *fractional* fluctuation amplitude decreases as $L^{-1/2}$). Our results are in agreement with this prediction.

Finally, our samples inadvertently contained a considerable concentration of magnetic impurities, which have a strong and very interesting effect on the fluctuations, especially at low applied magnetic field. We present two models to describe this behavior.

II. THEORETICAL BACKGROUND

A. Beenakker and van Houten formulation

In 1988, Beenakker and van Houten[7] provided a fully quantitative theory that included both the amplitude and the field scale of the QCF. Their calculation was performed for samples with $W,t \ll L_\varphi$ and $L \gg L_\varphi$, where W is the sample width and t is its thickness. Their central result is for the autocorrelation function $F(\Delta H) \equiv \langle \Delta R(H) \Delta R(H+\Delta H) \rangle$, where R is the sample resistance, H is the applied field, and the average is over all measured fields:

$$F(\Delta H)=R^4 6\left[\frac{e^2}{h}\right]^2\left[\frac{L_\varphi(\Delta H)}{L}\right]^3 \times\left[1+\frac{9}{2\pi}\left[\frac{L_\varphi(\Delta H)}{L_T}\right]^2\right]^{-1}, \quad (1)$$

where $L_T\equiv(\hbar D/k_BT)$ is the thermal length, D is the diffusion constant, and, for $l\ll W$,

$$L_\varphi(\Delta H)=\left[\frac{1}{L_\varphi^2}+\frac{1}{3}\left[\frac{\pi eW\Delta H}{h}\right]^2\right]^{-1/2}. \quad (2)$$

For strong spin-orbit scattering, the right-hand side of Eq. (1) should be multiplied[2,8] by $\frac{1}{4}$. This equation is correct to within 10% for all $L_T<L$. The characteristic field scale for the QCF, H_c, can be found by setting $F(\Delta H=H_c)=\frac{1}{2}F(\Delta H=0)$, and solving iteratively for H_c. (This expression of the Beenakker and van Houten results is only correct if the amplitude of the resistance fluctuations is much less than R. This is almost always the case, and is certainly the case for the samples used for this research.)

Equation (1) contains as complete a description of the fluctuations as is possible. The rms amplitude is given by $\Delta R_{\rm rms}=\{\langle[\Delta R(H)]^2\rangle\}^{1/2}=[F(\Delta H=0)]^{1/2}$. Expressing this in terms of the sheet resistance $R_\square$ to bring out the dimensional dependences, we have

$$\Delta R_{\rm rms}=\sqrt{6}R_\square^2\frac{e^2}{h}\frac{L^{1/2}L_\varphi^{3/2}}{W^2}\left[1+\frac{9}{2\pi}\left[\frac{L_\varphi(H)}{L_T}\right]^2\right]^{-1/2}. \quad (3)$$

Again, for strong spin-orbit scattering, the right-hand side should be multiplied by $\frac{1}{2}$.

B. Magnetic scattering

According to present theories,[2] paramagnetic scattering only affects QCF via the magnetic spin-flip scattering length L_s and its effect on L_φ:

$$L_\varphi=(L_i^{-2}+2L_s^{-2})^{-1/2}, \quad (4)$$

where L_i is the inelastic diffusion length, which reflects electron-phonon and electron-electron interactions. L_s is expected to depend on the magnetic field, though most workers in the closely related field of weak localization have intentionally restricted their measurements to low enough fields that L_s is constant. At low fields, the magnetic scatterers have random dipole orientations and are free to undergo spin-flip interaction with the conduction electrons, decreasing L_φ, and thus reducing the amplitude of the QCF. At high fields, all the magnetic scattering centers should align with the field, the randomness should be eliminated, and the amplitude of the QCF should increase.

In 1987, Benoit and co-workers[9] published data on the field dependence of the amplitude of the periodic AB oscillations. They measured three samples. Two were gold rings doped with differing concentrations of manganese, a paramagnetic scatterer. The third was also a gold ring, but with a paramagnetic salt adsorbed on the surface. They proposed a simple model of paramagnetic scattering to explain their results. They assumed that only the lowest two magnetic energy levels of the magnetic scatterers in their samples would be important, so that the scatterers could be treated as having spin $\frac{1}{2}$. Furthermore, the phase-breaking effect of the magnetic scatterers was assumed to be proportional to the probability of a scatterer being in two different states at two different times, so that the magnetic scattering rate would be proportional to $S=AP_uP_d$, where A is a coupling constant, and P_u and P_d are the probabilities of the scatterer being in the up or down state. We have

$$P_m=\frac{e^{g\mu_BmH/k_BT}}{e^{(1/2)g\mu_BH/k_BT}+e^{-(1/2)g\mu_BH/k_BT}}, \quad (5)$$

where $m=\pm\frac{1}{2}$ for spin up or down. Thus

$$S=\frac{1}{4}\frac{A}{\cosh^2(g\mu_BH/2k_BT)}. \quad (6)$$

(Here, we have included the factor of $\frac{1}{4}$ omitted by Benoit *et al.*) Using standard diffusion theory, they showed that, if magnetic scattering is the dominant phase-breaking process, then

$$L_\varphi=\left[\frac{la^3}{d^2Sc}\right]^{1/2}, \quad (7)$$

where l is the elastic mean free path, a is the atomic spacing, b is a characteristic length for magnetic interactions (of order a few atomic spacings), and c is the atomic fraction of magnetic scatterers. The derivation of this formula ignores a number of factors of order unity, but these can easily be absorbed by A and b.

This theory gave a fairly good description of their data, using reasonable parameter values. The data on the salt-covered sample was well described throughout the measured temperature range. However, they only published data at one temperature for the AuMn sample, so the model has not yet been thoroughly tested for magnetic scattering in the sample interior, and it has not been applied to any aperiodic fluctuation data.

C. Time dependence

Al'tschuler and Spivak,[10] and Feng *et al.*[11] pointed out that, in the case of two-dimensional diffusion ($t<l$), a given electron which diffuses through a sample visits every scattering site once, on the average. As they showed, this surprising fact has important implications for the MF: if even a single scattering site is moved a distance comparable to the Fermi wavelength, the entire interference pattern of the sample, and so the MF, will be changed substantially. Feng *et al.* also suggested that this effect might be used to observe the atomic motion associated with two-level systems in amorphous materials. However, in practice, at least for metallic samples, this effect can only be clearly observed in short (~1 μm) samples, such as that used by Meisenheimer and Giordano.[12] (A short sample allows high sensitivity, due to the good

electronic heat sinking, and the high allowable measuring current which results.)

In our samples, the diffusion is three dimensional ($t \gg l$). In this case, the size of the resistance change produced by a single moving scatterer is reduced by $(l/t)^{1/2}$, compared to two-dimensional diffusion. A rough calculation, using the approximation formula for the density of two-level systems given by Feng *et al.*, shows that the combined effect of the motion of all the two-level systems in our shortest sample ($R = 2.3$ kΩ) at 50 mK would amount to a change in resistance of ~ 1 mΩ, which is well below our experimental resolution at 50 mK. Thus we do not expect to see any effects from atomic motion.

III. EXPERIMENTAL TECHNIQUES

Our samples were patterned using lift off electron-beam lithography, following the procedure described by Mackie and Beaumont,[13] as presented by Rooks *et al.*[14] $Pd_{80}Si_{20}$ was chosen for the sample material because it is known to form the amorphous phase very readily,[15] and is well characterized.[16] The samples were deposited onto oxidized silicon wafers by ion-beam sputtering from a composite target consisting of strips of 99.998% pure Pd sheet[17] on a background of electronic-grade undoped Si plate.[18] They were passivated *in situ* with a 40-Å layer of SiO_x deposited from a target of semiconductor-grade quartz.[19]

The composition of the samples was measured by inductively coupled plasma (ICP) emission spectroscopy,[20] microprobe, energy dispersive spectroscopy, and Rutherford backscattering. All of these methods indicated that the films were 79–85 at. % Pd. Transmission electron microscope (TEM) diffraction images, thin-film x-ray diffraction images, high-resolution TEM bright-field imaging, and resistivity measurements all confirmed that the films were amorphous. The average measured Si content of 22 at. % is within the amorphous-forming region[15] for bulk (splat-cooled) PdSi. Because our films were ion-beam sputtered, the amorphous-forming region should be even broader, virtually assuring the amorphousness of our films.

The $Pd_{80}Si_{20}$ wires discussed in this paper are summarized in Table I. Micrographs of sample 1 are shown in Figs. 1(a) and 1(b). This sample had four voltage probes, allowing us to measure several different lengths from 12 to 87 μm. The width of these subsections ranged from 130 to 140 nm. Samples 2 and 3 were codeposited. Sample 2 was a meander pattern with total length 1.05 mm and width 180 nm, and is shown in Fig. 2.

The concentration of trace elements in the samples was estimated from ICP and secondary-ion mass spectroscopy (SIMS). Due to difficulties in obtaining a reliable standard, the absolute concentrations of trace elements could only be measured to within a factor of 3, although the relative concentrations between samples could be measured to an accuracy of 30%. Table II shows our best estimates for the concentrations of Cr and Fe. The concentrations are relatively high; we presume that this material was sputtered off the walls of the ion gun and vacuum chamber. Not surprisingly, these magnetic scatterers had a dramatic and very interesting effect on the quantum coherence effects in our samples.

The samples were very stable; the resistance of a given sample changed by less than 1% between one cooldown and the next. However, the magnetofingerprint always changed between cooldowns, perhaps due to the electrical stress caused by loading the sample into the refrigerator. Magnetoresistance measurements were carried out between 50 mK and 6 K in an Oxford Instruments dilution refrigerator enclosed in a radio-frequency-shielded room. Sample resistance was monitored by a true four-probe circuit, which sensed changes relative to a standard. The measuring current was very carefully limited so as to cause negligible sample heating; 2 nA was used for our lowest temperature (50 mK) measurements. To achieve good sensitivity, we were forced to use very long averaging times; a typical magnetic field sweep took 12 h. To improve amplifier stability, the temperature and humidity inside the shielded room were regulated to ±1% per 12-h period.

IV. BACKGROUND EFFECTS

A. Resistance versus temperature

Figure 3 shows the $\Delta R/R$ versus T curve for sample 1. This figure is a mosaic of several different traces, which

TABLE I. Sample dimensions and resistances.

Sample	Length (μm)	Width (nm)	Thickness (nm)	R (kΩ) at 4 K	$R_\square$ (Ω) at 77 K	ρ (μΩ cm) at 77 K
1	86.5	130	25	18.0	27.1	67.5
	49.5	126		10.6		
	24.6	133		5.03		
	12.4	144		2.32		
2	1050	180	24	211	37.8	90.0
	520	180		105		
3	92.9	207	24	17.0	37.8	90.0
4	72.1	169	26	12.6	29.5	76.7
	48.9	172		8.40		
	24.5	174		4.15		

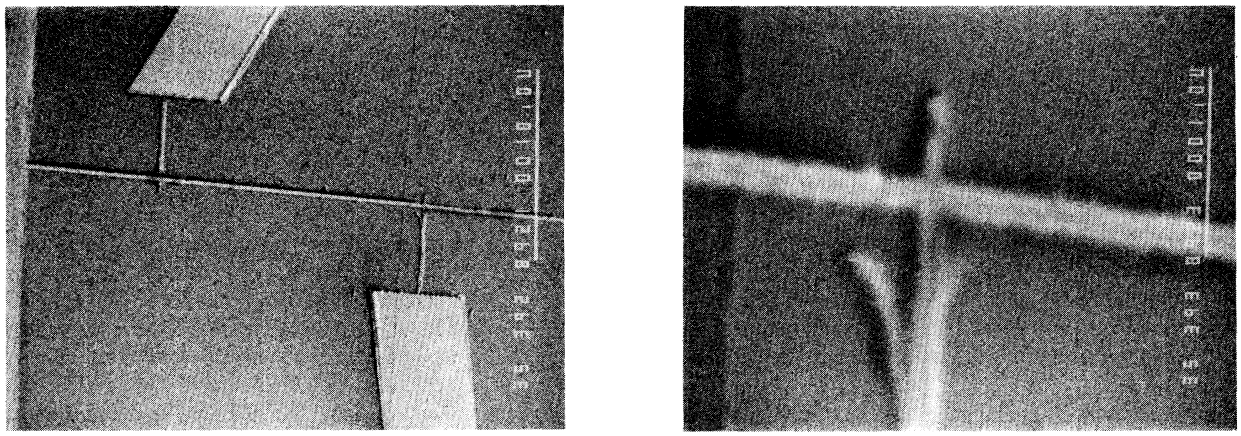

(a) (b)

FIG. 1. Scanning electron micrographs of sample 1, taken at an angle of 60° from normal along the length of the sample. (a) The bright bar in the upper right represents 10 μm. (b) The bar represents 1 μm.

accounts for the varying noise level. We will consider four principal contributions to the temperature dependence of the resistance: weak localization (WL), electron-phonon (e-ph) scattering, electron-electron (e-e) interaction, and Kondo effect. We will show that the effects of WL are fairly small. The contributions from e-ph scattering and e-e interaction can be estimated from known parameters. So, we will subtract these two effects out from the data, and fit the remaining temperature dependence to the Kondo theory.

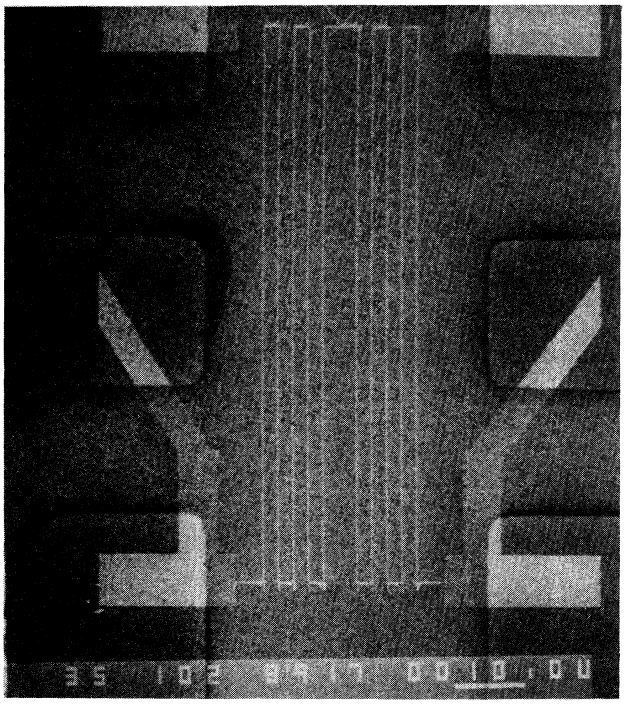

FIG. 2. Scanning electron micrograph of sample 2. The sample is a meander pattern with a total length of 1.05 mm and linewidth of 180 nm. The bright bar in the lower right represents 10 μm.

1. *Weak localization*

The contribution of WL is given by[21]

$$\frac{\Delta R(H=0,T)}{R} = \frac{1}{2}\frac{e^2}{h}\frac{\rho}{\pi}\left[\frac{3}{L_2}-\frac{1}{L_3}\right], \tag{8}$$

where ρ is the resistivity. The sensitivity to temperature comes from the temperature dependence of the two characteristic lengths L_2 (the "triplet" length) and L_3 (the "singlet" length), which are defined by[22]

$$L_2 \equiv (L_i^{-2}+\tfrac{4}{3}L_{\text{s.o.}}^{-2}+\tfrac{2}{3}L_s^{-2})^{-1/2} \tag{9}$$

and

$$L_3 \equiv (L_i^{-2}+2L_s^{-2})^{-1/2}, \tag{10}$$

where L_i is the diffusion length between inelastic scattering event, $L_{\text{s.o.}}$ is the spin-orbit diffusion length, and L_s is the magnetic scattering diffusion length. Equation (8) is valid for the case of three-dimensional (3D) localization, i.e, $L_2, L_3 \ll W, t, L$. (See below for a further discussion

TABLE II. Estimated Fe and Cr concentrations from ICP and SIMS measurements. Although the relative concentrations between samples are accurate to within 30%, the absolute concentrations are only correct to within a factor of 3.

Sample	Approximate absolute concentration (atomic percent) Fe	Cr
1	0.08	0.02
2	0.2	0.02
3	0.2	0.02
4	0.2	0.06

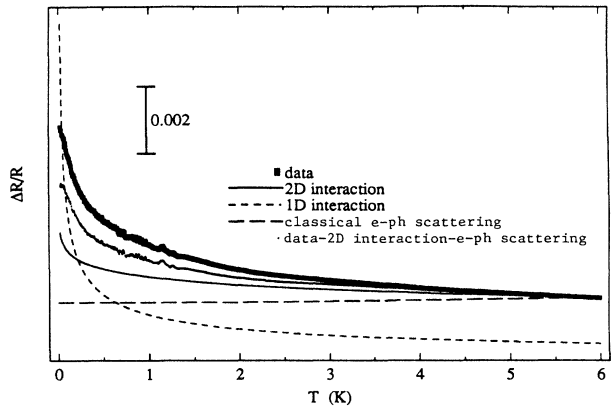

FIG. 3. Subtraction of interaction and classical e-ph scattering effects from $\Delta R/R$ vs T curve for sample 1 ($R=18$ kΩ). The data shown are taken from several different traces, which accounts for the varying noise level. The 2D interaction theory is valid for $T \gg 0.22$ K, while the 1D theory is valid for $T \ll 0.22$ K. (The zeros for the corresponding curves, which are arbitrary, have been adjusted so they cross at 0.22 K.) Above 50 mK, where we can be sure there are no heating effects, the raw data do not vary as sharply as the 1D theory. Therefore we assume the transition to 1D is not completed until below 50 mK, and subtract out only the 2D theory, and the classical e-ph scattering.

of sample dimensionality.) These lengths are usually determined by fitting magnetoresistance (MR) measurements to weak localization theory. But, as we will see, the low-temperature MR of our samples appears to be strongly influenced by the Kondo effect, preventing such a fit. However, we can make rough estimates for the lengths, and use them to show that the contribution of weak localization to the R versus T curve is small. By careful comparison with other experiments,[23] and using the results of the QCF analysis below, we estimate that, at 50 mK, $L_2 \approx 4$ nm and $L_3 \approx 11$ nm. Thus our samples are indeed in the 3D limit throughout the experimental temperature range. (Note: this is the dimensionality at low fields, where weak localization is important. We will show below that our samples become 1D at high fields.) Making reasonable assumptions[22,24–26] for the temperature dependence of L_i, we then estimate that the total effect of weak localization from 6 K to 50 mK would be $\Delta R/R \approx 2\times 10^{-4}$, which amounts to about 4% of the observed change. We will neglect this contribution, since we are unable to reliably calculate it in detail.

2. Electron-phonon scattering

When electrons scatter off phonons, their momentum, as well as their energy, is changed. This creates additional resistance, which decreases as the temperature is lowered. At low temperatures, e-ph scattering contributes $\Delta\rho=\delta T^2$ to the resistivity of bulk $Pd_{80}Si_{20}$, where[27] $\delta=2.8\times 10^{-4}$ $\mu\Omega$ cm/K^2. Although the phonon spectrum of a thin film, and so δ, is likely to be somewhat different from that for the bulk, the total contribution from this effect is a small one, and so the bulk value should serve as an adequate approximation. We can subtract this contribution out before analyzing the remaining terms. (See below.)

3. Electron-electron interaction

The effects of e-e interaction depend on the dimensionality of the sample relative to the thermal length $L_T \equiv (\hbar D/k_B T)^{1/2}$. For 2D e-e interaction (i.e., $t \ll L_T \ll L, W$) we have[21,28]

$$\frac{\Delta R(H=0,T)}{R} \cong -\frac{R}{\pi}\frac{e^2}{h}\ln\left[\frac{k_B T\tau}{h}\right] \tag{11}$$

for the case of strong spin-orbit scattering ($\hbar\tau_{\text{s.o.}}^{-1} \gg k_B T$). For 1 D e-e interaction (i.e., $t, W \ll L_T \ll L$), we have

$$\frac{\Delta R(H=0,T)}{R} \cong 2\sqrt{2}\frac{e^2}{h}R\frac{L_T}{W} . \tag{12}$$

To find L_T, we need D. We use the free-electron approximation, which works quite well[27,29] in $Pd_{80}Si_{20}$. Thus we have

$$D = \tfrac{1}{3}v_F l = \frac{h^2}{4me^2}\frac{1}{k_F\rho} . \tag{13}$$

The average result for the Si content of our films was 22 at. %. Mitzutani and Massalski[15] found $k_F=1.4$ Å^{-1} for this case. Thus, for sample 1, we estimate $D=5.0$ cm^2/sec.

Using this value of D, we find that $L_T=W$ at $T=0.22$ K for the 87-μm section of sample 1. Therefore there should be 2D interaction for $T \gg 0.22$ K, and 1D interaction for $T \ll 0.22$ K. Figure 3 shows both the 1D and the 2D theories, along with the raw data. Even at the lowest temperature for which the data are completely trustworthy (50 mK), the sample has not completed the transition to 1D behavior; the 1D theory predicts a stronger temperature dependence than is observed. This behavior is not unreasonable; at 50 mK, L_T is only a little more than twice the sample width. Therefore, as an approximation, we subtract out the 2D theory over the entire temperature range, as well as e-ph scattering effects discussed in Sec. IV A 2, as shown in Fig. 3.

4. Kondo effect

We attribute the temperature dependence remaining after the above subtraction of e-e and e-ph effects to Kondo effect. We estimate that, for any Kondo temperature $T_K < 15$ K, both the width and the thickness of our samples are smaller than η_K, the Kondo screening radius. However, Bergmann[30] has found experimentally that the effects of such reduced dimensionality are actually quite small (at least for 2D samples: $t \ll \eta_K \ll W, L$). So, since there is as yet no full, quantitative theory for samples with dimensions less than η_K, we will use the 3D theory:[31]

$$\frac{\Delta R}{R}=\frac{1}{k_F\rho}\frac{h}{e^2}\frac{c}{z}\left[1-\frac{\ln(T/T_K)}{[\ln^2(T/T_K)+\pi^2S(S+1)]^{1/2}}\right], \tag{14}$$

where c is the concentration (atomic fraction) of the magnetic scatterers, S is their spin, and z is the number of conduction electrons per host atom. Using the free-electron model, we estimate $z=1.3$ for our samples. $S=\frac{3}{2}$ for both[27,32] Fe and Cr in $Pd_{80}Si_{20}$.

The best fit to the data for sample 1 using (14) is for a scatterer concentration of 0.23 at. %, with a Kondo temperature of 0.22 K. The agreement with theory is excellent, as shown in Fig. 4. Recall from the ICP and SIMS measurements that we estimated the total concentration of Fe and Cr in this sample to be ~0.1 at. % (see Table II), but that, although the relative concentrations between samples were fairly well determined, the absolute concentration was uncertain up to a factor of 3. The best fit value of 0.23 at. % lies well within this range. However, we note that the theory is rather insensitive in the experimental temperature range to the value of T_K; very good fits (with rms deviation from the data equal to only about 2.5% of the total observed change in R) can also be obtained for T_K ranging from 30 mK to 1.5 K, with c equal to or less than about 0.3 at. % (the maximum allowable, based on the SIMS and ICP results). Similar fits can be performed for the other samples. Using the results of the trace element analysis as a rough guide, our best estimates are $c\approx0.2$ at. % for sample 1, $c\approx0.5$ at. % for samples 2 and 3, and $c\approx0.4$ at. % for sample 4. The Kondo temperatures cannot be very closely determined: T_K is likely between 30 mK and 20 K for all the samples, although there is some indication that it may be in the low end of this range (say, less than 1.5 K) for sample 1, and slightly higher (say, more than 2 K) for samples 3 and 4. We will see in Sec. IV B that these findings agree with the relative size of the background MR and the relative field scale of the magnetoresistance for our samples.

B. Background magnetoresistance (Ref. 33)

We consider four contributions to the background: classical MR, *e-e* interaction, WL, and Kondo effect.

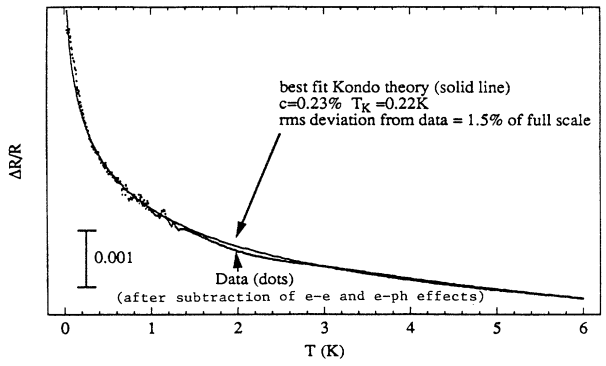

FIG. 4. Kondo theory fit to $\Delta R/R$ vs T curve for sample 1.

Typically, the classical MR for amorphous metals is negligible compared to the other terms.[16] Electron-electron interactions only affect the MR for[28] $g\mu_B H \gg \hbar/\tau_{s.o.}, \hbar/\tau_s$. As discussed above, our best estimate for $L_{s.o.}$ in our samples is approximately 5 nm. This implies that we would require $H \gg 100$ T to observe MR effects from *e-e* interaction.

Because WL is strongly influenced by magnetic scattering, there is an intimate connection between WL and the Kondo effect. Unfortunately, there is as yet no theory incorporating the Kondo effect into WL that is valid near or below T_K. As discussed above, the analysis of the R versus T data, as well as the analysis of the conductance fluctuations (see below), suggests that $T_K \geq 1$ K. A detailed interpretation of our background MR is thus impossible at this time. However, we can explain most of the background features qualitatively.

Figure 5 shows the background MR for samples 1 and 4 as a function of temperature. The traces shown are not MF's. They are an average of all available data, which includes a number of different resistance fluctuations for each sample. These different resistance fluctuations were available due to accidental electrical shocks delivered to the sample, which caused rearrangement of the scatterers, as discussed below. This averaging was performed to eliminate the fluctuations and display the background MR as clearly as possible.

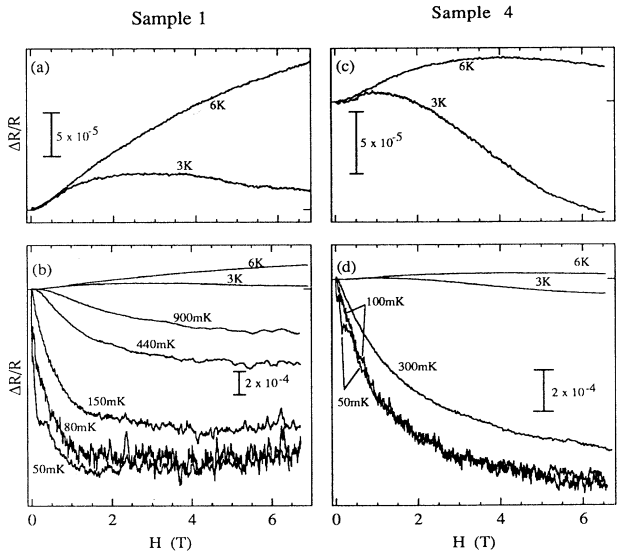

FIG. 5. Background magnetoresistance (MR) curves for various temperatures for samples 1 and 4. These are not magnetofingerprints. Each trace is an average of all available data for each sample, including a number of different magnetofingerprints, and data from all subsections. This averaging was performed to suppress the resistance fluctuations and to display the background MR as clearly as possible. For each sample, the upper graph shows an enlarged view of the MR at 3 and 6 K. Note that each of the four graphs has a different vertical scale.

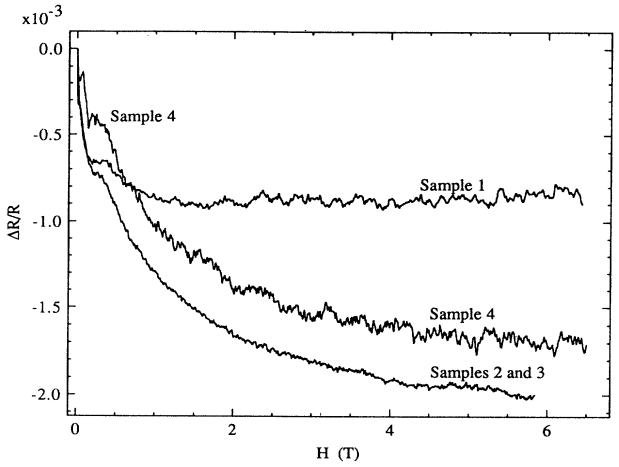

FIG. 6. Background MR at 50 mK for three samples. As in Fig. 5, these are not magnetofingerprints, but rather they are averages of all available data. The backgrounds of 2 and 3 were assumed to be the same, since they were codeposited. This was, in fact, observed experimentally. So, the raw MR traces of these two samples were averaged together to produce the background shown.

The shape of the 6-K MR curves at low field is quite reminiscent of WL in the strong spin-orbit scattering limit. However, no fit could be obtained for reasonable parameter values, presumably because the WL theory does not include the Kondo effect. At higher fields, especially at lower temperatures, the resistance decreases, which one does not expect from WL. We attribute this drop in resistance to the alignment of magnetic scatterers with the field, which decreases the magnetic scattering rate.

As the temperature is lowered further this effect of "freezing out" the magnetic scatterers becomes more and more striking. At the very lowest temperature, 50 mK, a shoulder develops at about 0.5 T. We believe this to be a feature of the background, rather than the fluctuations, since it was observed in all of our samples (Fig. 6). This shoulder may be an indication that there are two species of magnetic scatterers in our samples (perhaps the Fe and the Cr), which have two different effective magnetic moments. At 50 mK, one species appears to have a characteristic field of about 0.1 T, while the other has a characteristic field of about 1 T. The behavior at 50 and 150 mK appears to be almost totally determined by the freeze-out of magnetic scatterers.

Figure 6 shows the background MR at 50 mK for all the samples. We expect $\Delta R/R \propto c$ for dilute scatterers. Thus, if the contribution from WL is negligible, the change in resistance from $H=0$ to the field at which the background levels off should be proportional to the total scatterer concentration. This ratio for samples 1:3:4 is 2:5:4, which is identical to the ratio we estimated from the combined ICP, SIMS, and R versus T results, 0.2%:0.5%:0.4%.

V. FLUCTUATION EFFECTS

A. Magnetoresistance fluctuations

Figure 7 shows the MR of sample 1 (87-μm section) at 50 mK. Two traces are shown, one taken as the field was swept up and the other as it was swept down. They are identical to within the resolution of our measurement. This figure clearly demonstrates that the quantum coherence effects which give rise to the magnetofingerprint remain operative in the extreme diffusion limit of an amorphous metal.

One striking feature is that the rms size of the fluctuations is not constant; it increases as the field is increased, first becoming noticeable at ~ 2 T, and reaching a plateau which begins at roughly 4 T. We believe this low-field suppression is due to magnetic scattering, as will be discussed in more detail below. This behavior is qualitatively similar to that observed by Benoit *et al.*[9] in AuMn, and to the total suppression of structure at $H < 0.4$T observed by van Haesendonck *et al.* in AuFe.[34]

Figure 8(a) shows a MF for sample 2 ($L=1.05$ mm) at 50 mK. In this sample, the amplitude of the fluctuations is reduced compared to what might have been expected based on sample 1, even at the highest fields and lowest temperatures at which we could make measurements. We attribute this to a stronger effect of the magnetic scatterers in this sample; this theory is supported by the SIMS analysis (see Table II), which showed that this sample had a concentration of Fe roughly twice that of sample 1, and by the ΔR versus T results, which indicated that the total concentration of magnetic scatterers was roughly 2.5 times that of sample 1. The suppression of structure cannot be attributed to the sample's large

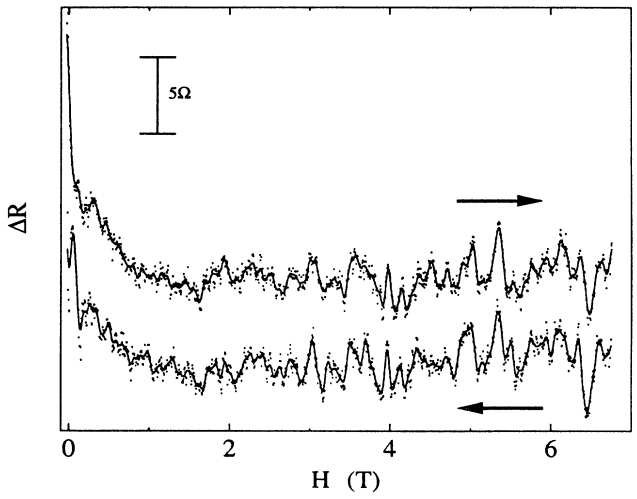

FIG. 7. MR traces for the 87-μm section of sample 1 ($W=130$ nm, $R=18$ kΩ), taken at 50 mK with a measuring current of 2 nA. The dots are the raw data, and the solid line is a digitally filtered version to aid in comparing the traces. (The raw data were used for all quantitative analysis.) Because of the long averaging times required, each sweep took roughly 12 h.

length, because sample 3, which was cosputtered with sample 2, showed a similar suppression. In any case, the high-field portion of the MR [Fig. 8(b)] shows clearly reproducible structure. This figure demonstrates that, indeed, magnetofingerprints are not limited to mesoscopic samples, but can also be observed in samples which are macroscopically long. Because of the small amount of data for this sample, we cannot be sure whether or not the rms amplitude of the fluctuations was still increasing at 7 T.

B. Stability

These MF's usually remained reproducible for at least a few days. On very rare occasions (perhaps twice over about 4 months of measuring time), we observed apparently spontaneous changes in resistance, which were accompanied by a complete change of the MF. The size of the jumps was roughly the same size as the amplitude of the structure in the MF; this is much too large to be caused by a single moving scatterer. Possibly, each of these jumps was the result of a chain-reaction cascade of atomic motion. More likely, they were due to electrical transients of which we were unaware, but which were large enough to get through our filtering. Similar irreversible jumps in the resistance, accompanied by changes in the MF, have been observed by Birge *et al.*[35]

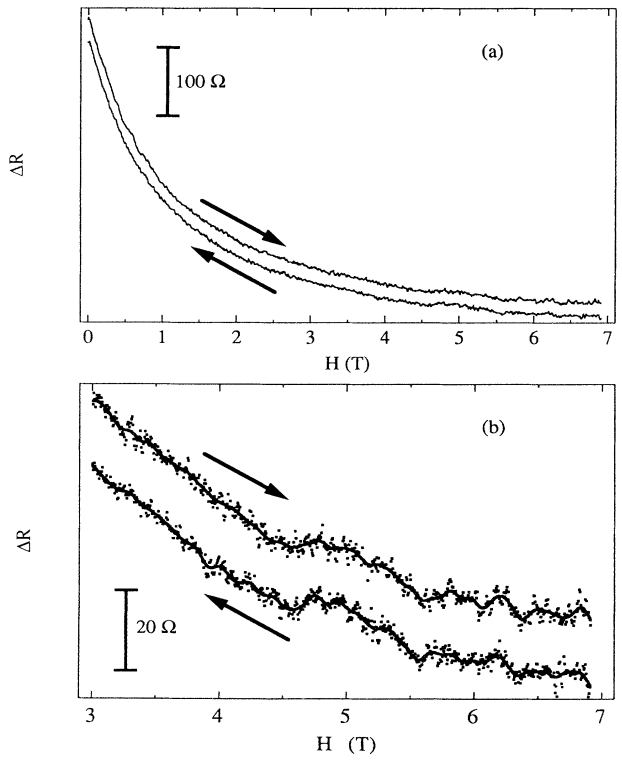

FIG. 8. MR traces for sample 2 (1.05 mm×180 nm, $R=211$ kΩ). (a) MR over the field range 0–7 T. (b) Closeup of high-field data. The small squares are the raw data, and the solid line is a digitally filtered version to aid in comparing the traces.

C. Field and temperature dependence of the fluctuations

Figure 9(a) shows the average size of the fluctuations for sample 1 as a function of field at 50 mK. This figure was produced by averaging data from all of the available fingerprints for this sample, as well as data from each of its subsections. As discussed above, Benoit *et al.*[9] observed qualitatively similar behavior for the h/e oscillations in a gold ring with magnetic scatterers. The theory they used to describe their results was based on the assumption that, since they only took data at a low temperature, only the lowest two magnetic energy levels of the magnetic scatterers in their samples would be important, so that the scatterers could be treated as having spin $\frac{1}{2}$. Furthermore, they assumed that magnetic scattering was the dominant phase-breaking mechanism throughout their field range 0–2 T. These assumptions will not hold for our experiments, which extend over a wider tempera-

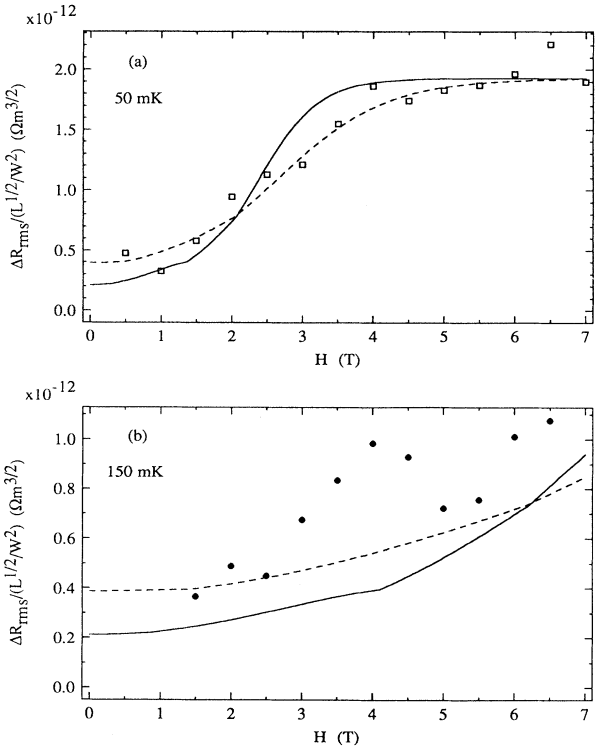

FIG. 9. $\Delta R_{\rm rms}$ [normalized by dividing by $(L^{1/2}/W^2)$] vs H for sample 1. (a) 50 mK. The dashed line shows the best fit, using (15), and requiring $L_i=165$ nm, as determined from the amplitude of the high-field fluctuations. The best fit parameters are $L_s=44$ nm and $\mu_{\rm eff}=0.29\mu_B$. The solid line shows another fit, which is also in fairly good agreement with the data ($L_s=16$ nm and $\mu_{\rm eff}=0.50\mu_B$). (b) 150 mK: fits using the L_s and $\mu_{\rm eff}$ from the 50-mK fit, but allowing L_i to vary, with the constraint that $L_i(150\ {\rm mK})\le L_i(50\ {\rm mK})$. The best fits shown here were obtained for $L_i(150\ {\rm mK})=L_i(50\ {\rm mK})$; for any known form of inelastic scattering, one expects $L_i(150\ {\rm mK})\le 0.7L_i(50\ {\rm mK})$. Neither fit matches the 150-mK data.

ture range (50 mK–0.9 K) and field range (up to 7 T).

We can generalize the Benoit *et al.* theory to the simplest form of $S=\frac{3}{2}$ scatterers (both the Fe and the Cr have[27,32] spin $\frac{3}{2}$ in $Pd_{80}Si_{20}$) and to include the effects of nonmagnetic phase breaking. We assume the simplest model for $S=\frac{3}{2}$ scatterers, i.e., a Zeeman splitting equal to gmH, where $m=\pm\frac{3}{2},\pm\frac{1}{2}$. Furthermore, we assume, as do Benoit *et al.*, that the magnetic scattering rate is proportional to the probability of a magnetic scatterer being in two different states at two different times. We find

$$L_\varphi=\left[L_i^{-2}+\tfrac{4}{3}L_s^{-2}\left[\frac{1}{\cosh\alpha}+\frac{1}{\cosh\alpha+1}\right]\right]^{1/2} \quad (S=\tfrac{3}{2}), \qquad (15)$$

where $\alpha=g\mu_B H/k_B T$, L_s is the magnetic scattering diffusion length at $H=0$, and L_i is the phase-breaking diffusion length for nonmagnetic processes. By using this field-dependent L_φ in (2) and (3), we obtain a complete theory for the amplitude of the fluctuations as a function of field.

The situation becomes somewhat more complicated if L_φ changes from being smaller than W at low fields to being larger than W at high fields. Equation (3) is correct for $L_\varphi \gg W$ (i.e., the 1D case). For $L_\varphi \ll W$ (i.e., the 2D case), we may correct (3) by multiplying the right-hand side by $(W/L_\varphi)^{1/2}$. More specifically, it is a reasonable assumption that this dimensional crossover follows the same behavior as the 2D to 1D weak-localization crossover. For this case,[24] the 1D form is quantitatively correct for $L_\varphi > 1.3W$, while the 2D form is quantitatively correct for $L_\varphi < 0.5W$. We assume that the dimensional crossovers occur for the same L_φ/W ratios in our case, and, as a rough approximation, make a simple linear interpolation in the regime in between. For some of our data, L_φ actually passes through two-dimensional crossovers, since it becomes less than the thickness of our samples at the lowest fields. We use similar assumptions to deal with the 3D to 2D transition, substituting t for W.

Inspection of the data in Fig. 9(a) indicates that the amplitude of the fluctuations becomes approximately constant above ~ 4 T. Assuming that the magnetic scattering is completely frozen out in this range, and that the amplitude of the fluctuations is thus determined by L_i, we can use the amplitude of the fluctuations to measure L_i, via (3). This yields $L_i=165$ nm at 50 mK for sample 1. In principle, we could use a similar procedure to find L_s, using the amplitude of the low-field fluctuations. However, this amplitude is so small that such a determination would be very uncertain, so we have chosen to leave L_s as a free-fitting parameter. The dashed line in Fig. 9(a) shows the best fit to the 50-mK data, with best fit parameters $L_s=44$ nm and $\mu_{\rm eff}\equiv gS\mu_B=0.29\mu_B$. The match to the data is excellent. The solid line shows the theoretical prediction for $L_s=16$ nm and $\mu_{\rm eff}=0.50\mu_B$, which also matches the data fairly well. This figure is quite reminiscent of the data presented by Benoit *et al.* at 160 mK.

Benoit *et al.* presented no data at other temperatures; we have measurements of the fluctuations up to 0.9 K. The dashed line in Fig. 9(b) shows the predictions of our theory for 150 mK, using the L_s and $\mu_{\rm eff}$ determined by the best fit at 50 mK, while the solid line shows the predictions of the second parameter set. In both cases, we allowed L_i to vary to find the best fit, with the restriction that it should be equal to or smaller than the 50-mK value of 165 nm. In both cases, the best fit was found for 165 nm (the upper bound), but neither of these theoretical curves matches the data very well.

We can obtain an important clue to the explanation for this discrepancy by examining the $\Delta R_{\rm rms}$ versus H curves over our entire temperature range, Fig. 10(a). (For the higher temperatures, we could not determine the low-field values for $\Delta R_{\rm rms}$, since the characteristic field of the fluctuations at high temperatures and low fields was so large that we were unable to separate the fluctuations from the background with digital filtration. We consider the data that are shown to be reliable.) In Fig. 10(b), we have adjusted the y scale for each curve so that the curves intersect at 6.5 T. This figure reveals the surprising fact that, although the overall amplitude of the fluctuations is suppressed as the temperature is increased, *the characteristic field required to freeze out the magnetic scattering is nearly temperature independent,* at least up to 440 mK. As was shown in Fig. 9, this is in strong contrast to the very nonlinear temperature dependence predicted by (15).

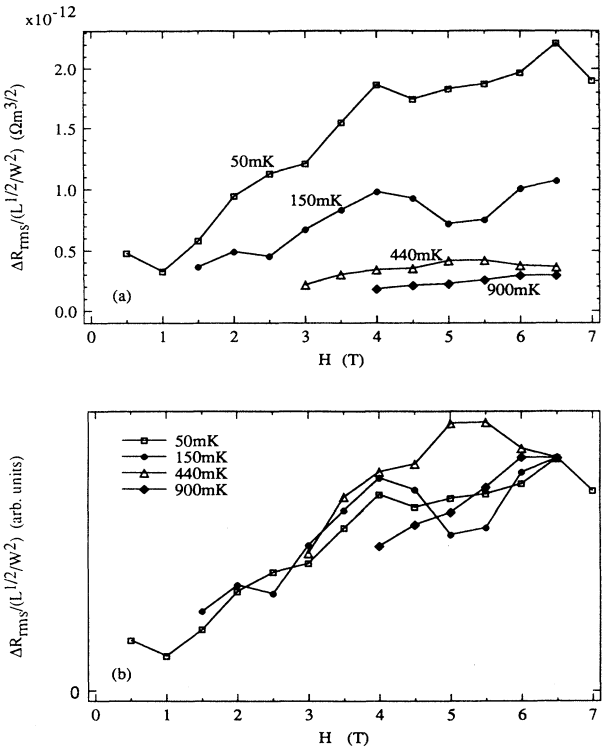

FIG. 10. $\Delta R_{\rm rms}$ vs H for sample 1 at various temperatures. (a) Measured values. (b) Y scale for each temperature adjusted so the curves intersect at 6.5 T.

These results can be explained by allowing μ_{eff} to be temperature dependent, with $\mu_{\text{eff}} \propto T$ below 440 mK. This is a possible consequence of the Kondo effect. Well below the Kondo temperature, the conduction electrons screen the magnetic scatterers, thus decreasing their effective magnetic moments. This should not only decrease the magnetic scattering rate τ_s^{-1}, as Bergmann and co-workers have observed experimentally,[30,36,37] but also μ_{eff}. If this is the mechanism responsible for the temperature dependence of μ_{eff}, then we expect

$$\tau_s^{-1} \propto L_s^{-2} \propto \mu_{\text{eff}} \propto T^p , \tag{16}$$

where p might equal 2, as predicted by the Fermi liquid theory;[37,38] 1, as observed experimentally by Bergmann;[36] or $\frac{1}{2}$, as observed by Peters *et al.*[7] As mentioned, Fig. 10(b) indicates $p \approx 1$, at least at low T.

The solid lines in Fig. 11(a) show the predictions of allowing μ_{eff} and L_i to vary, but assuming that the only temperature dependence of L_s is through μ_{eff}. (Here, we are using the second parameter set from 50 mK; the best-fit 50-mK parameter set does not produce curves which agree with this high-T data.) At 150 mK, we find good agreement with the assumption that $\mu_{\text{eff}} \approx T$. At 440 mK, the μ_{eff} we find is smaller than predicted by a linear T dependence, but we still find a fairly good fit. At 900 mK, we must allow L_s to have additional temperature dependence in order to find a good fit; the parameters shown were found by allowing L_i, L_s, and μ_{eff} to vary freely. This may be an indication that 900 mK is close to T_K; it is observed experimentally[37] that the reduction of the magnetic scattering rate begins at $T \approx T_K/2$. So, it may be that $T_K \approx 1-2$ K for this sample; this estimate agrees with the range of most likely Kondo temperatures from the R versus T measurements: 30 mK–1.5 K. This T_K is also in agreement with results of thermopower measurements[39] on Fe in PdSi.

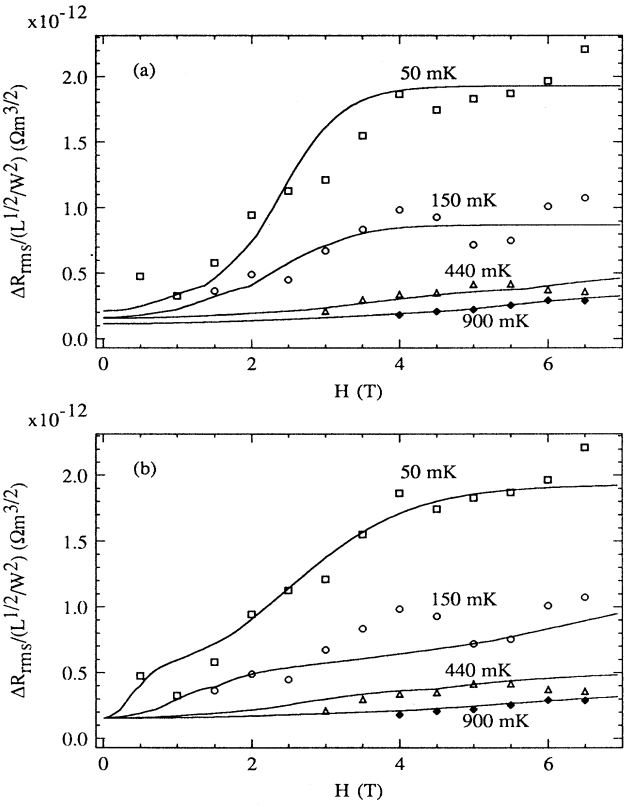

FIG. 11. Two models to explain the observed behavior of ΔR_{rms} vs H for sample 1. (a) Single magnetic scatterer species, with temperature-dependent μ_{eff}. The parameters are as follows. 50 mK: $L_i = 165$ nm, $L_s = 16$ nm, $\mu_{\text{eff}} = 0.29\mu_B$; 150 mK: $L_i = 76$ nm, $L_s = 9.5$ nm, $\mu_{\text{eff}} = 1.5\mu_B$; 440 mK: $L_i = 50$ nm, $L_s = 9$ nm, $\mu_{\text{eff}} = 1.7\mu_B$; 900 mK: $L_i = 41$ nm, $L_s = 5$ nm, $\mu_{\text{eff}} = 3.1\mu_B$. (b) Two species of scatterers, each with fixed μ_{eff}. One species has $L_s = 6$ nm and $\mu_{\text{eff}} = 2.6\mu_B$, while the other has $L_s = 70$ nm and $\mu_{\text{eff}} = 0.23\mu_B$.

To summarize, the behavior of the fluctuations as a function of field is consistent with a Kondo screening which produces a temperature-dependent magnetic moment. The moment appears proportional to T for $T \leq 150$ mK. The screening of the magnetic moment is reflected not only in the magnetic scattering rate, but also in a temperature-dependent μ_{eff}. We estimate T_K for sample 1 to be 1–2 K.

Another explanation for the apparent temperature dependence of μ_{eff} is that there may be two populations of magnetic scatterers, each with fixed μ_{eff}. At low temperatures, the high-μ_{eff} population would be frozen out at very low fields, so the observed field dependence would reflect the lower-μ_{eff} population. At high temperatures, the lower-μ_{eff} population would never be frozen out at experimentally accessible fields, so the observed field dependence would reflect the higher-μ_{eff} population. Thus the observed μ_{eff} would appear to increase with temperature. Figure 11(b) shows the results of this model, assuming $L_i \propto T^{-1/2}$, as indicated by the amplitude of the high-field fluctuations (see below). The best fit parameters are $L_s = 6$ nm and $\mu_{\text{eff}} = 2.6\mu_B$ for scatterer population number 1, and $L_s = 70$ nm and $\mu_{\text{eff}} = 0.23\mu_B$ for population 2. The agreement is good over the entire temperature regime. Since the concentration $c \propto \tau_s^{-1} \propto L_s^{-1}$, the values of L_s obtained from the fit correspond to a ratio of 3.4 between the concentration of population 1 and that of population 2. This agrees well with the results of the ICP and SIMS analysis, where ratio of 4 was found (see Table II).[40] (Here we have made the tentative assignment that population 1 corresponds to Fe and population 2 to Cr.) The characteristic field for aligning spin-$\frac{3}{2}$ scatterers is $3k_BT/\mu_{\text{eff}}$. At 50 mK, this corresponds to 0.087 T for population 1 and 0.96 T for population 2. Recall that a qualitative examination of the 50-mK MR suggested that there might be two scatterer species, with characteristic fields of roughly 0.1 and 1 T, respectively; these values agree well with the two-population model.

For both models, the best-fit parameters are of reasonable magnitude, although there are too many of them to have any confidence in the exact values. The correct physical explanation for our data is likely a combination of the two effects, i.e., Kondo effect and a variety of mag-

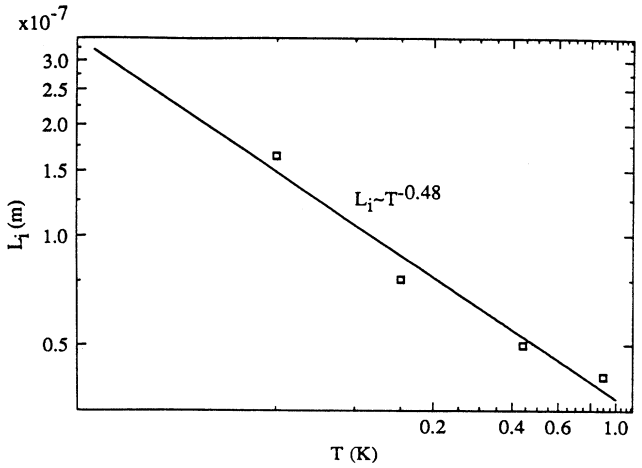

FIG. 12. Temperature dependence of L_i as determined from the amplitude of the high-field resistance fluctuations for sample 1. Squares, data; solid line, best fit.

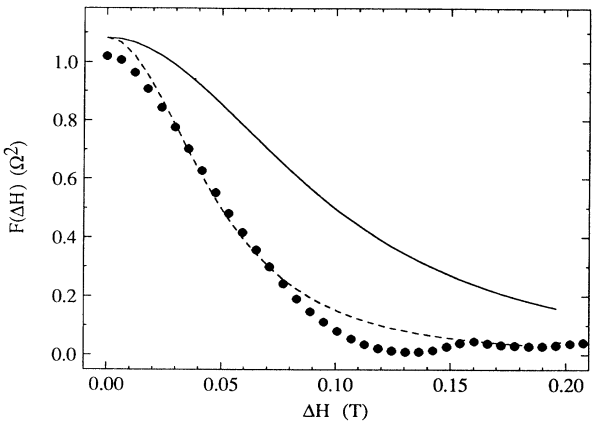

FIG. 13. Autocorrelation function $F(\Delta H)\equiv\langle R(H)R(H+\Delta H)\rangle$ of the 87-μm section of sample 1 for small H in the range 4–7 T. The solid line shows the predictions of (1)–(3). The dashed line shows what happens if the H scale of the theory is divided by 2.

netic scatterer populations. Although in this case our conclusions cannot be made entirely quantitative, the above analysis shows the usefulness of quantum conductance fluctuations; we have used them to measure L_φ as a function of H. In contrast, analysis of background magnetoresistance using weak-localization theory can only determine L_φ at $H=0$.

Figure 12 shows the temperature dependence of L_i for sample 1, as measured from the high-field amplitude of the fluctuations. We find $L_i \propto T^{-1/2}$, which corresponds to 2D *e-e* scattering. This finding is consistent with our $R(T)$ results.

D. Autocorrelation function

As discussed in Sec. V C, for sample 1 at 50 mK, $\Delta R_{\rm rms}$ is approximately constant in the field range 4–7 T. Figure 13 shows the autocorrelation function $F(\Delta H)\equiv\langle \Delta R(H)\Delta R(H+\Delta H)\rangle$ for the data on the 87-μm section in this regime. Using (3), the $\Delta R_{\rm rms}$ for this field range yields $L_\varphi=165$ nm. Inserting this into (1) and (2), we obtain a detailed prediction for the autocorrelation function, shown by the solid line of Fig. 13. The field scale for the theoretical prediction differs from the data by almost exactly a factor of 2. (The dashed line shows what happens if we divide the H scale of the theory by 2.)

This level of agreement between the field scale as predicted from $\Delta R_{\rm rms}$ and the measured field scale has generally been considered good in the field of quantum conductance fluctuations (see, e.g., Ref. 35). However, we believe the discrepancy to be outside the range of experimental scatter.

The reason for this discrepancy may be that Eqs. (1)–(3) are strictly valid only for $L_\varphi \gg W$, whereas in our case, $W\cong 1.3L_\varphi$. Thus our sample is just barely narrow enough to be in the 1D WL regime.[24] However, the criterion for one dimensionality with respect to the Beenakker and van Houten theory [Eqs. (1)–(3)] may be somewhat different than that for WL.

Another possible explanation is that there is some mechanism reducing the amplitude of the fluctuations in our sample below that given by (3). If this were the case, then the actual L_φ in our samples would be larger than 165 nm. This larger L_φ would cause the theoretical field scale to be smaller, and more in tune with our observations. One possibility for this reduction mechanism is a much higher density or activity of two-level systems than we have estimated. Another might be some interplay between the Kondo effect and quantum conductance fluctuations. (The connection between the two has not yet been addressed quantitatively.)

A third possibility for the discrepancy lies in the vale of L_T, which we obtained from the bulk value of k_F using the free-electron model. However, L_T (or k_F) would have to be off by more than a factor of 2 to explain the observed discrepancy.

E. Length dependence of the fluctuations

According to the theory of stochastic averaging, the amplitude of the resistance fluctuations should *increase* as the sample length is increased: $\Delta R_{\rm rms} \propto L^{1/2}$ [see (3)]. To data, this prediction had only been checked up to $L \approx 6L_\varphi \approx 4$ μm for metallic samples.[5] Our data extend the range for which the theory can be checked by three orders of magnitude.

Since $\Delta R_{\rm rms} \propto L^{1/2}$, a plot of $(\Delta R_{\rm rms})^2$ versus L should yield a straight line, if W is constant. However, the width of our samples varied slightly. So, examination of (3) shows that we should plot $(\Delta R_{\rm rms})^2 W^4$ versus L for sample 1, for which $W<L_\varphi$, and $(\Delta R_{\rm rms})^2 W^3$ versus L for samples 2 and 3, for which $W>L_\varphi$. [Recall that, for this case, the right-hand side of (3) should be multiplied by

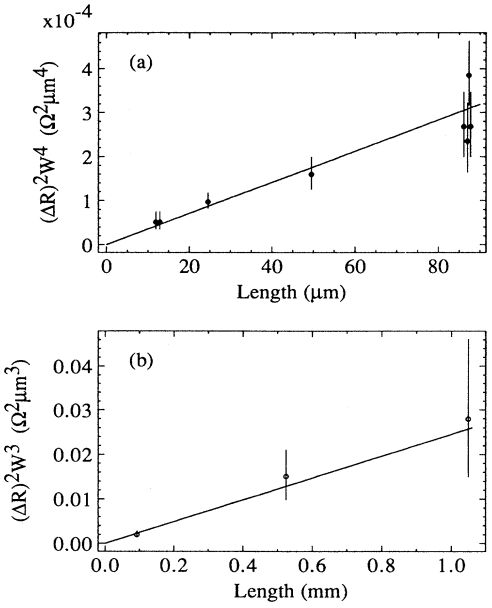

FIG. 14. Length dependence of the resistance fluctuation amplitude. (a) The various subsections of sample 1. In this case, $L_\varphi > W$, so we have compensated for the slight variations in width between the subsections by multiplying by W^4 [see (3)]. (b) Samples 2 and 3. These samples were codeposited, and so should have the same L_i and L_s. For these samples, $L_\varphi < W$, so we have multiplied by W^3.

$(W/L_\varphi)^{1/2}$.]

Figure 14(a) shows the plot for the various subsections of sample 1, which should all have the same L_s and L_i, and thus can be compared quantitatively. As mentioned previously, due to accidental electrical shocks delivered to the sample, we were able to measure more than one magnetoresistance fluctuation for some of the subsections. In these cases, the points have been slightly displaced horizontally so they can be seen. These data are in excellent agreement with the $L^{1/2}$ prediction; the straight line shown corresponds to $L_\varphi = 165$ nm.

Figure 14(b) shows the plot for samples 2 and 3, which were codeposited, and so should have the same L_s and L_i. Again, there is good agreement with the theory of stochastic averaging. The line shown corresponds to $L_\varphi = 90$ nm.

Thus we have checked the $L^{1/2}$ prediction fairly carefully out to $L/L_\varphi \cong 500$ with sample 1, and have verified it somewhat less quantitatively (because of the larger error bars) all the way out to $L/L_\varphi \cong 12\,000$ with samples 2 and 3.

VI. SUMMARY

We have fabricated amorphous PdSi thin films using ion-beam sputtering from a composite target. The amorphousness of the films was carefully verified by four different techniques. We patterned the films using electron-beam lithography into wires with linewidths less than 200 nm: one of them was over 1 mm long. The resistance and magnetoresistance of the wires was measured at temperatures down to 50 mK, using a measuring current which was carefully limited to avoid heating the sample.[41]

The resistance versus temperature traces of our samples can be quantitatively described by a combination of electron-phonon scattering, two-dimensional electron-electron scattering, and Kondo effect. The concentrations of magnetic scatterers determined by the Kondo fits is consistent with measurements of the levels of Fe and Cr in our films, using inductively coupled plasma spectroscopy and secondary-ion mass spectroscopy.

The background magnetoresistance is qualitatively explained by a combination of weak localization and Kondo effect. There is, as yet, no theory combining these effects that is valid near or below the Kondo temperature T_K, so a quantitative description of the MR is impossible. However, the total change in resistance from 0 to 7 T for our four main samples is consistent with the Fe and Cr concentrations, which we estimated from the combined ICP, SIMS, and R versus T results.

The principal results of this research are on quantum conductance fluctuations. Our measurements of aperiodic, reproducible structure in the MR of amorphous samples show that the quantum coherence effects that give rise to the magnetofingerprints remain operative even in the limit of maximum disorder. We observed MF's even for our 1-mm-long sample, and checked the stochastic averaging prediction $\Delta R_{\rm rms} \propto L^{1/2}$ out to $L/L_\varphi \approx 12\,000$, extending the regime for which this relation has been verified by three orders of magnitude.

The amplitude of the fluctuations increased with field. We attribute this behavior to alignment of the magnetic scatterers by the field. With (3), we used the amplitude of the fluctuations to measure the phase-breaking diffusion length L_φ as a function of magnetic field. These measurements indicate that, at 50 mK, the magnetic scattering rate decreased by at least a factor of 16 as the field was increased from 0 to 4 T. Simple paramagnetic scattering predicts[42] a change of, at most, 1.7; the failure of this theory is consistent with our estimation that our resistance-fluctuation measurements were made below the Kondo temperature.

We developed a model, not only for the overall change in the amplitude of the fluctuations from zero field to high field, but also for the shape of the $\Delta R_{\rm rms}$ versus H curve. This model was based on that presented by Benoit *et al.*,[9] modified to include the effects of nonmagnetic phase breaking and to allow for the simplest type of $S = \frac{3}{2}$ scatterers. To fit our data over the entire temperature range, we were forced to include the effects of Kondo screening by allowing both the effective magnetic moment and the zero-field magnetic scattering rate τ_s^{-1} to vary as a function of temperature. We required $\tau_s^{-1} \propto \mu_{\rm eff}$. This model explains our results at 440 mK and below very well. By 900 mK, it no longer agrees with the data, perhaps because 900 mK is too close to T_K. (To obtain a good fit at 900 mK, we had to allow $\mu_{\rm eff}$ and τ_s^{-1} to vary independently.) Thus we estimated $T_K \approx 1$–2 K, in

agreement with the R versus T data.

A second model, assuming two magnetic scatterer populations, each with fixed μ_{eff}, also describes the data well, and is qualitatively supported by the background MR and the ICP and SIMS analysis.

From the high-field amplitude of the fluctuations, we measured the nonmagnetic phase-breaking diffusion length L_i as a function of temperature. We found an approximate relation $L_i \propto T^{-1/2}$, which is characteristic of 2D e-e scattering. The R versus T results also indicated that the e-e scattering was likely 2D throughout our temperature range.

We also used the high-field amplitude of the fluctuations to predict the characteristic field scale (at high field), using the theory of Beenakker and van Houten.[7] The prediction was larger than the experimental field scale by a factor of 2. Possible explanations include a much higher density and activity of two-level systems than we estimated, a sample width too close to L_φ, or a failure of the theory to account correctly for strong spin-orbit scattering in the presence of aligned Kondo scatterers.

ACKNOWLEDGMENTS

This work was supported by the National Science Foundation, under Grants No. DMR89-12927 and No. DMR86-14003. We gratefully acknowledge the assistance of Neil M. Zimmerman, who performed microprobe analysis of our films, and helpful discussions with C. W. J. Beenakker, Shechao Feng, P. Santhanam, Frans Spaepen, A. Douglas Stone, Sean Washburn, and Richard A. Webb.

*Present address: Department of Physics, University of Texas, Austin, TX 78712.

†Present address: Department of Physics, University of Minnesota, Minneapolis, MN 55455.

‡Present address: Department of Physics, Center for Superconductivity Research, University of Maryland, College Park, MD 20742.

[1]R. A. Webb, S. Washburn, C. P. Umbach, and R. B. Laibowitz, in *Localization, Interaction, and Transport Phenomena,* edited by B. Kramer, G. Bergmann, and Y. Bruynseraede (Springer-Verlag, Berlin, 1984); C. P. Umbach, S. Washburn, R. B. Laibowitz, and R. A. Webb, Phys. Rev. B **30**, 4048 (1984); G. Blonder, Bull. Am. Phys. Soc. **29**, 535 (1984).

[2]See, for example, P. A. Lee, A. D. Stone, and H. Fukuyama, Phys. Rev. B **35**, 1039 (1987).

[3]For an excellent review, see S. Wahsburn and R. A. Webb, Adv. Phys. **35**, 375 (1986).

[4]W. J. Skocpol, P. M. Mankiewich, R. E. Howard, L. D. Jackel, D. M. Tennant, and A. D. Stone, Phys. Rev. Lett. **56**, 2685 (1986); **58**, 2347 (1987).

[5]A. Benoit, C. P. Umbach, R. B. Laibowitz, and R. A. Webb, Phys. Rev. Lett. **58**, 2343 (1987).

[6]M. A. Howson and B. L. Gallagher, Phys. Rep. **170**, 265 (1988).

[7]C. W. J. Beenakker and H. van Houten, Phys. Rev. B **37**, 6544 (1988).

[8]B. L. Al'tschuler and B. I. Shklovskii, Zh. Eksp. Teor. Fiz. **91**, 220 (1986) [Sov. Phys.—JETP **64**, 127 (1986)]; S. Feng, Phys. Rev. B **39**, 8722 (1989); A. D. Stone, *ibid.* **39**, 10736 (1989); and (private communication).

[9]A. Benoit, S. Washburn, C. P. Umbach, R. A. Webb, D. Mailly, and L. Dumoulin, in *Anderson Localization,* edited by T. Ando and H. Fukuyama (Springer-Verlag, Berlin, 1988), p. 346.

[10]B. L. Al'tschuler and B. Z. Spivak, Pis'ma Zh. Eksp. Teor. Fiz. **42**, 363 (1985) [JETP Lett. **42**, 447 (1985)].

[11]S. Feng, P. A. Lee, and A. D. Stone, Phys. Rev. Lett. **56**, 1960 (1986); **56**, 2722(E) (1986).

[12]T. L. Meisenheimer and N. Giordano, Phys. Rev. B **39**, 9929 (1989).

[13]S. Mackie and S. P. Beaumont, Solid State Technol. **28**, 117 (1985).

[14]M. T. Rooks, P. McEuen, S. Wind, and D. E. Prober, *Science and Technology of Microfabrication,* MRS Symposia Proceedings No. 76 (Materials Research Society, Pittsburgh, 1987), p. 55.

[15]U. Mitzutani and T. B. Massalski, Phys. Rev. B **21**, 3180 (1980).

[16]*Amorphous Metallic Alloys,* edited by F. E. Luborsky (Butterworths, London, 1983).

[17]Johnson Matthey Chemicals Ltd., Orchard Rd., Royston, Hertfordshire SG8 5HE, England.

[18]Crystal Systems Inc., Shetland Industrial Park, 35 Congress St., Salem MA 01970.

[19]United States Fused Quartz Co, Inc., 17 Madison Rd., Fairfield NJ 07006.

[20]Inductively coupled plasma spectroscopy performed by the Laboratory for Special Analysis, Randolph MA 02368.

[21]See, for example, M. Olivier, J. O. Strom-Olsen, Z. Altounian, R. W. Cochrane, and M. Trudeau, Phys. Rev. B **33**, 2799 (1986).

[22]See, for example, G. Bergmann, Phys. Rep. **107**, 1 (1984), and references therein.

[23]R. S. Markiewicz and C. J. Rollins, Phys. Rev. B **29**, 735 (1984).

[24]P. Santhanam, S. Wind, and D. E. Prober, Phys. Rev. B **35**, 3188 (1987).

[25]A. B. Pippard, Philos. Mag. **46**, 1104 (1955); J. M. Ziman, *Electrons and Phonons* (Clarendon, Oxford, 1960), p. 213.

[26]B. L. Al'tschuler, A. G. Aronov, D. E. Khmel'nitskii, and A. I. Larkin, in *Quantum Theory of Solids,* edited by I. M. Lifshitz (Mir, Moscow, 1982); B. L. Al'tschuler, A. G. Aronov, and D. E. Khmel'nitskii, J. Phys. C **15**, 7367 (1982).

[27]R. Hasegawa, Ph.D. thesis, California Institute of Technology, 1968.

[28]P. A. Lee and T. V. Ramakrishnan, Rev. Mod. Phys. **57**, 287 (1985).

[29]See, for example, R. C. Crewdson, Ph.D. thesis, California Institute of Technology, 1966.

[30]G. Bergmann, Phys. Rev. Lett. **57**, 1460 (1986).

[31]See, for example, J. Kondo, in *Solid State Physics,* edited by F. Seitz, D. Turnbull, and H. Ehrenreich (Academic, New York, Vol. 23, 1969), p. 183; K. Fischer, in *Springer Tracts in*

Modern Physics, edited by G. Hohler (Springer Verlag, Berlin, 1970), Vol. 54.

[32]R. Hasegawa, J. Appl. Phys. **41**, 4096 (1970).

[33]Unfortunately, the concentration of magnetic impurities we estimate for our samples does not lie clearly either in the spin-glass or the isolated impurity (Kondo) limit. There is, as yet, no complete theory that includes the effects of both Kondo scattering and weak localization. The situation is further complicated by a number of dimensional transitions as the field and temperature are varied. Even simplified versions of the theory include many fitting parameters, more than we can pin down with our limited set of measurements, which were directed primarily at the magnetofingerprints. Thus, to simplify the matter somewhat, we will ignore the effects of interactions between the magnetic scatterers throughout the remainder of this paper. This is obviously a gross approximation, but all the data can be at least qualitatively explained without recourse to scatterer interaction. It is possible that the Kondo screening of the magnetic moments acted to diminish the interactions considerably. Clearly, in a future study, it would be desirable to use a better characterized Kondo system, with a lower concentration of scatterers.

[34]C. van Haesendonck, H. Vloeberghs, Y. Bruynseraede, and R. Jonckheere, in *Nanostructure Physics and Fabrication,* Proceedings of the International Symposium, College Station, Texas, 1989, edited by M. A. Reed and W. P. Kirk (Academic, Boston, 1989), p. 467.

[35]N. O. Birge, B. Golding, and W. H. Haemmerle, Phys. Rev. Lett. **62**, 195 (1989).

[36]G. Bergmann, Phys. Rev. Lett. **58**, 1236 (1987).

[37]R. -P. Peters, G. Bergmann, and R. M. Mueller, Phys. Rev. Lett. **60**, 1093 (1988).

[38]P. Nozieres, J. Low Temp. Phys. **17**, 31 (1974).

[39]P. Svoboda and P. Vasek, J. Phys. F **15**, 2489 (1985).

[40]It is difficult to extract even a rough estimate for the concentration ratio from the background MR.

[41]For further experimental details, see W. F. Smith, Ph.D. thesis, Harvard University, 1989.

[42]W. Wei, G. Bergmann, and R. -P. Peters, Phys. Rev. B **38**, 11 751 (1988).

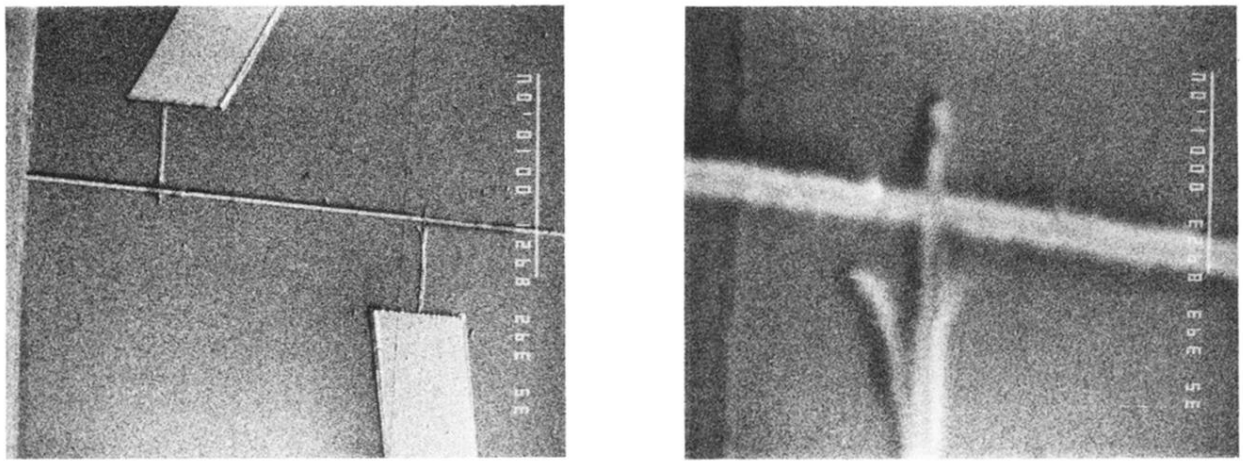

(a) (b)

FIG. 1. Scanning electron micrographs of sample 1, taken at an angle of 60° from normal along the length of the sample. (a) The bright bar in the upper right represents 10 μm. (b) The bar represents 1 μm.

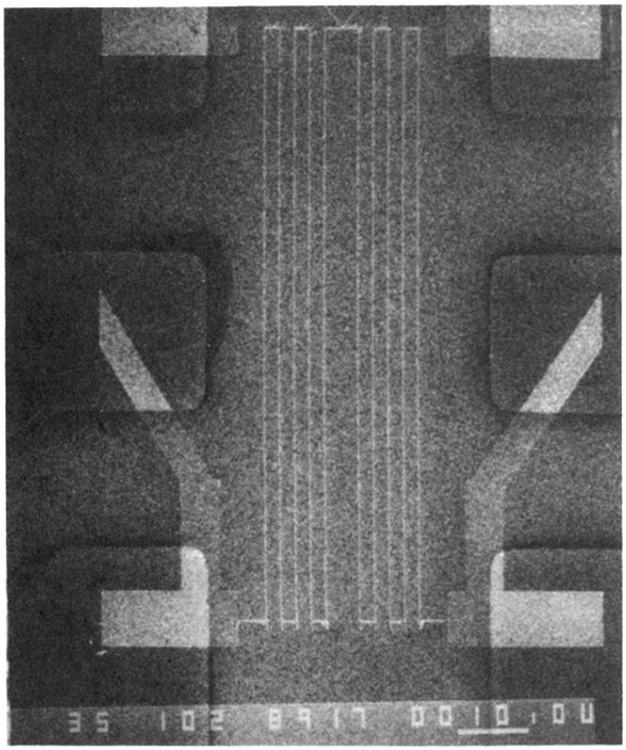

FIG. 2. Scanning electron micrograph of sample 2. The sample is a meander pattern with a total length of 1.05 mm and linewidth of 180 nm. The bright bar in the lower right represents 10 μm.